JOURNAL OF GUIDANCE, CONTROL, AND DYNAMICS
Vol. 18, No. 1, January–February 1995

Validation of Finite-Dimensional Approximate Solutions for Dynamics of Distributed-Parameter Systems

John L. Junkins* and Sangchul Lee†
Texas A&M University, College Station, Texas 77843

An inverse dynamics method is introduced for constructing exact special-case solutions for hybrid coordinate ordinary/partial systems of differential equations (hybrid ODE/PDE systems). The solution is constructed such that it lies near a given approximate numerical solution, and therefore the special-case solutions can be generated in a versatile and physically meaningful fashion and can serve as a benchmark problem to validate approximate solution methods. The exact solution is constructed such that it is a differentiable, continuous-function neighbor of the given approximate numerical solution. This continuous solution is then substituted into the governing system of ODEs/PDEs and a full complement of distributed and boundary forces is determined algebraically to exactly satisfy the differential equations. This process has been automated by computer symbol manipulation. Since the exact special-case algebraic solutions can be evaluated anywhere in space and time, this approach is ideally suited to providing a true exact motion and the corresponding forces for studying the convergence errors in a family of approximate solutions. This methodology makes it possible for one to rigorously determine exact solution errors for a significant class of ODE/PDE systems for which the initial-value problem is not, in general, exactly solvable. We explore the utility of this method in validating numerical solution methods.

Introduction: Construction of Benchmark Problems for Solution of Ordinary Differential Equations

GIVEN a flexible multibody dynamic system, most rigorously described by a hybrid system of nonlinear ordinary and partial differential equations (ODEs/PDEs), we seek to validate simulations of the behavior of the system by numerical methods. With most applications of approximate-solution algorithms, we must somehow evaluate the accuracy of a given approximate solution without knowing the true solution. What happens if we can construct an exact forced-response solution for a special-case motion near (in a sense to be established) a candidate approximate solution? This gives us an absolute standard and promises the capability of displaying exactly the space/time distribution of solution errors for the special-case solution and therefore suggests remedies, if needed, to improve the discretization-based solution process.

The idea is easily introduced by first considering the initial-value problem for nonlinear ODEs.[1] In general, we do not know the true solution and the numerical methods give us an approximate solution. The most common way of assessing the true error of a numerical solution is to reduce the tolerance, integrate again, and compare the results.[2,3] Although more sophisticated error analyses can be conducted, there is no general way to absolutely guarantee the final accuracy of the solutions. Whereas this does not preclude obtaining practical solutions for most applications, it remains very difficult to answer subtle questions. In view of the historical and recent developments, we observe that the theory of differential equation solvers is far from complete, so that the understanding of a given code's performance invariably requires a study of experimental results. Hull et al.[4] and Krogh[5] provided two outstanding collections of test problems for this purpose for the case of ODEs. These test problems have been used in the development and testing of the codes and can be regarded as standard benchmark problems for initial-value problem solvers. Whenever we know the true solution of a test problem, we can investigate the relationship between the true, or global, error and parameters of a given code (e.g., step size, local error tolerance, and order). Of course, only for a small minority of interesting problems can the initial-value problem be solved analytically. For these cases where the true solution is unknown, we introduce here an inverse method that algebraically constructs a continuous neighbor of a given numerical approximate solution. The neighboring continuous motion does in fact exactly satisfy the differential equations (with a known small forcing function) and serves as an excellent benchmark problem since the benchmark problem is a customized near neighbor of the problem of interest.

The remaining and most critical question is: How useful is the convergence and accuracy information obtained for the benchmark problem as regards drawing conclusions for the original problem? It is important to recall that the benchmark problem includes a known small forcing function to the original problem. If the perturbation is small enough, it is to be expected that all derivatives will be close for the two problems and, consequently, the behavior of standard discrete-variable methods will be similar with respect to both accuracy and stability. It is certainly true that there are open questions on this issue needing further investigation; however, by constructing a family of neighboring benchmark problems, it is usually possible to judge the size of the neighborhood in which the convergence and accuracy properties are relatively invariant with respect to the perturbation and thereby gain the practical insight needed to proceed with confidence in a solution process and associated error measures. Several applications[1] provide strong evidence supporting the practicality of this approach.

Now, we propose a method to construct a benchmark problem that is a closely neighboring trajectory of a given approximate solution of the original problem. As will be evident, the benchmark problem motion is constructed algebraically so that it satisfies exactly the differential equation but with a known, usually small, time-varying forcing function. We can then investigate the global error/parameter relationship of the benchmark problem with the true solution in hand. Under the assumption that the original problem is well posed with respect to small perturbations, we have valuable information about the optimal parameters and the accuracy of the numerical solution. Through study of a family of neighboring benchmark problems, we can directly establish insight on the "stability" of this error analysis.

Initially, we restrict attention to nonlinear ODE systems; we subsequently broaden the discussion and examples to consider hybrid differential equation systems. Here we introduce one way for

Received Aug. 23, 1993; revision received April 20, 1994; accepted for publication April 20, 1994.

*George J. Eppright Chair Professor, Department of Aerospace Engineering. Fellow AIAA.

†Graduate Student, Department of Aerospace Engineering. Student Member AIAA.

constructing the exact benchmark problem. First we consider the following initial-value problem for a second-order ODE system:

$$\ddot{x} = f(x, \dot{x}, t), \qquad x(t_0) = x_0,$$
$$\dot{x}(t_0) = \dot{x}_0 \qquad \text{over} \qquad t_0 \le t \le t_f \tag{1}$$
$$f\colon R^N \times R^N \times R \to R^N$$

Here we consider the case where x is a scalar (i.e., $N = 1$). The following approach can be easily generalized for the vector case. A candidate discrete approximate solution can be obtained from the original second-order differential equation (1) using a numerical method. To establish a continuous, differentiable motion near a given approximate solution, we use a least-squares approximation based upon the discrete version of the Chebyshev polynomials; this polynomial approximation can be established directly from the discrete approximate solution.[6,7] We first consider the least-squares process. There are n data points such as $x_1 = g(t_1)$, $x_2 = g(t_2), \ldots, x_n = g(t_n)$, where t_i are the equally spaced values of the independent variable ($h_t = t_{i+1} - t_i = \text{const.}$)

Using conventional least-squares approximation techniques, we can construct an approximating function that passes arbitrarily close to these data. To avoid matrix inversion, we use orthogonal Chebyshev polynomials[8] to construct the approximation:

$$x = g(t) = G(\bar{t}) \equiv \sum_{i=1}^{m} a_i T_i(\bar{t}) \tag{2}$$

where $\bar{t}(t) = (t - t_1)/h_t$. The form of the approximation of Eq. (2) is not crucial, so long as the set of functions is complete and differentiable. In our case, we adopted Chebyshev polynomials $T_i(\bar{t})$ satisfying a discrete orthogonality condition so that the coefficient can be computed to arbitrary order from

$$a_j = \frac{\sum_{i=1}^{n} x_i T_j(\bar{t}_i)}{\sum_{i=1}^{n} T_j(\bar{t}_i) T_j(\bar{t}_i)}$$

where $1 \le j \le m$. Since no matrix inverse is required, and owing to the completeness of these polynomials, it is well known that most smooth functions can usually be approximated accurately using a modest degree (n).

We can find $g(t)$ from $G(\bar{t})$ since $g(t) = G(\bar{t}(t))$. Using this least-squares approximation, we can find a continuous, differentiable, analytical solution $x_b(t)$ that interpolates or lies very near the given n discrete numerical $\tilde{x}_i$ approximate solutions of Eq. (1). Of course this analytical expression $x_b(t)$ does not satisfy exactly Eq. (1). However, substituting $x_b(t), \dot{x}_b(t), \ddot{x}_b(t)$ into the equation $e(t) = \ddot{x}(t) - f(x(t), \dot{x}(t), t)$ allows us to determine an analytical function for the perturbation term $e(t)$ that appears in the following differential equation:

$$\ddot{x}(t) = f(x(t), \dot{x}(t), t) + e(t) \equiv F(x, \dot{x}, t) \tag{3}$$

Since $f(x(t), \dot{x}(t), t)$ is given and $e(t)$ is an available algebraic function, $F(x, \dot{x}, t)$ is available. Now $x_b(t)$ satisfies Eq. (3) exactly, and finally, this known function $x_b(t)$ is a neighbor of the original numerical solution $\{\tilde{x}_1, \tilde{x}_2, \ldots, \tilde{x}_n\}$. By algebraic construction the function $e(t) = \ddot{x}_b(t) - f(x_b(t), \dot{x}_b(t), t)$ is known analytically, and therefore we know this small forcing function at all t, and obviously, we know "how small" $e(t)$ is. This function is programmed and Eq. (3) can then be solved by numerical methods and the results can be compared to the known exact $x_b(t), \dot{x}_b(t)$. The above mathematical procedure can be performed successfully using computer symbol manipulation;[9] this is especially important for the generalizations to consider hybrid differential equations. Now Eq. (3) is a benchmark problem of Eq. (1) and $x_b(t), \dot{x}_b(t), \ddot{x}_b(t)$ satisfy Eq. (3) exactly. We obviously want the perturbation function $e(t)$ to be as small as possible; i.e., the benchmark problem is not only a near neighbor of the original discrete solution, but it also very nearly satisfies the given differential equations.

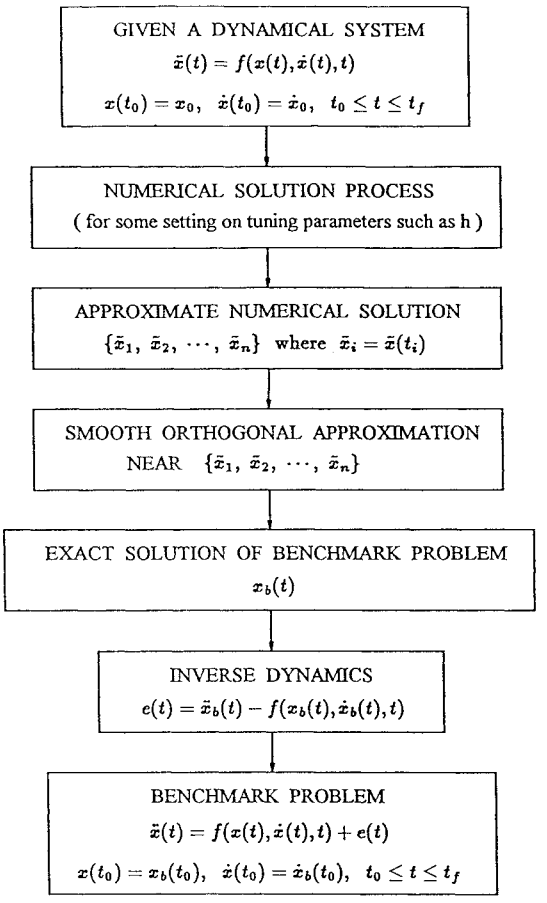

Fig. 1 Flow chart for construction of benchmark problem.

The previous least-squares approximation method has often been found to give poor results near the ends of the interval. This poor fit may cause a relatively large $e(t)$ near the initial and final times. To avoid this problem, we integrate Eq. (1) over the enlarged interval $t_{0-} \le t \le t_{f+}$ (where $t_{0-} < t_0$, $t_{f+} > t_f$) and use these numerical results as generators for analytical solutions over the original interval $t_0 \le t \le t_f$. Experience indicates that a 20% "enlargement" $[(t_{f+} - t_{0-}) \ge 1.2(t_f - t_0)]$ is almost always sufficient to support good interpolation over the original interval $t_0 \le t \le t_f$. If the measure of $e(t)$ is judged too large, then we increase the number of Chebyshev polynomials m to reduce $e(t)$ over the whole interval, or "start over" by attempting to find a better approximate numerical solution to initiate the process. Figure 1 provides a logical flow chart showing construction of a benchmark problem.

Now we demonstrate the idea using a simple nonstiff problem. We use the Runge-Kutta fourth-order method with fixed step size. Therefore we have the most common case that the integration control parameter is simply the step size h. The relationship between step size h and the global, or true, errors gives us the information about the critical value for h and the accuracy of the numerical solution. We consider the following nonlinear, nonautonomous, second-order differential equation:

$$\ddot{x} = -x - 0.1(1 + x^2)\dot{x} + 0.1x^3 + \sin 3t \tag{4}$$

where $x(0) = 1$ and $\dot{x}(0) = 0$, and we seek the solution over the interval $0 \le t \le 10$. We convert Eq. (4) to a first-order system as follows:

$$\dot{x}_1 = x_2\,, \qquad \dot{x}_2 = -x_1 - 0.1\left(1 + x_1^2\right)x_2 + 0.1x_1^3 + \sin 3t \tag{5}$$

where $x_1(0) = 1$ and $x_2(0) = 0$.

First, we solve Eq. (5) using the Runge-Kutta fourth-order method to evaluate the candidate discrete approximate solution. Here we use 121 data points over the 20% enlarged time interval $-1 \le t \le 11$. Second, we establish a continuous, differentiable, analytical expression for interpolating $x_{1_b}(t)$ from the discrete approximate solution

$\tilde{x}_1(t)$. We use a degree-30 Chebyshev polynomial approximation for the least-squares fitting. Finally we substitute $x_{1_b}(t)$, $\dot{x}_{1_b}(t)$, $\ddot{x}_{1_b}(t)$ into Eq. (4) and symbolically determine the function $e(t)$, which appears in the equation

$$\ddot{x} = -x - 0.1(1 + x^2)\dot{x} + 0.1x^3 + \sin 3t + e \tag{6}$$

To use the Runge-Kutta method, Eq. (6) can be converted to a first-order system as follows:

$$\dot{x}_1 = x_2, \qquad \dot{x}_2 = -x_1 - 0.1\left(1 + x_1^2\right)x_2 + 0.1x_1^3 + \sin 3t + e \tag{7}$$

Now, Eq. (6) serves as a benchmark problem for Eq. (4), because we know functions $x_b(t)$ and $e(t)$ that satisfy Eq. (6) exactly. Upon solving Eqs. (7) numerically with various values chosen for h and using the benchmark initial state as initial conditions $[x_1(0) = x_b(0), x_2(0) = \dot{x}_b(0)]$, we can establish the relationship between step size and global error. When we use the pointwise error in the root-mean-square sense, we are led to the results in Fig. 2, which shows the global error–step size relationship on a log-log scale. The rate of convergence on a log-log scale is 4 in this problem; this coincides with the fact that an rth-order method should have a global error of $\mathcal{O}(h^r)$ in the absence of arithmetic errors.[10] The critical value for step size is about 0.001; if h decreased below 0.001, then the results deteriorate due to the round-off error. To study the robustness of the convergence characteristics of Fig. 2, we introduce relatively large perturbations in the initial conditions and the nonautonomous term in the differential equation as follows:

$$\ddot{x} = -x - 0.1(1 + x^2)\dot{x} + 0.1x^3 + 1.2\sin 3t \tag{8}$$

where $x(0) = 1.2$ and $\dot{x}(0) = 0.2$ over the interval $0 \le t \le 10$.

After using the same procedure to vary the step size, we obtain the global error–step size relationship shown in Fig. 3. Notice that Figs. 2 and 3 are almost identical. In other words, both the critical value h and the associated accuracy are essentially unchanged, even though we introduced large (20%) perturbations in the initial conditions and in the forcing term of the differential equation. Obviously these results are problem dependent, but a similar process will provide the needed insight for other problems.

Now we apply this idea to an idealized three-body distributed-parameter system. The main difference is that there are two independent variables for space and time. Therefore, the least-squares approximation method must be generalized to deal with two independent variables. To obtain an approximate candidate discrete solution, we use a linear quadratic regulator (LQR) to design control forces and we use the finite element approach for space discretization. From this approximate solution, we construct a smooth, differentiable, analytical solution that is physically meaningful. We investigate the exact space-time distribution of errors of the numerical simulation using the Newmark method[11] with finite element modeling.

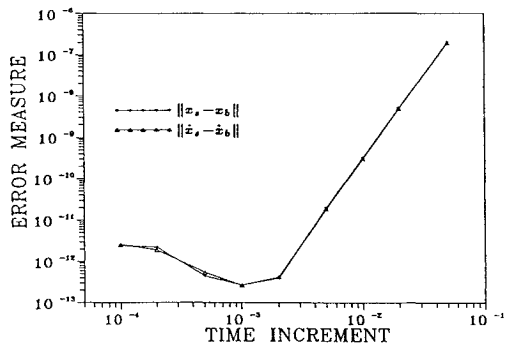

Fig. 2 Error measure vs time step size.

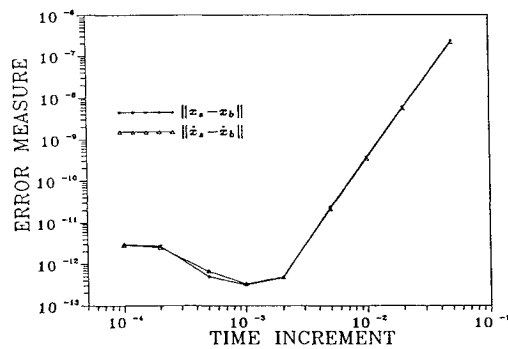

Fig. 3 Error measure vs time step size (perturbed case).

Three-Body Distributed-Parameter System

Now we demonstrate the idea on an idealized three-body distributed-parameter system. With reference to Fig. 4, we consider a rigid hub with a cantilevered flexible appendage that has a finite tip mass. Table 1 summarizes the configuration parameters of this flexible structure.

The appendage is considered to be a uniform flexible beam, and we make the Euler-Bernoulli assumptions of negligible shear deformation and negligible distributed rotatory inertia. The beam is cantilevered rigidly to the hub. Motion is restricted to the horizontal plane, and we neglect the velocity component $-y\dot{\theta}$ that is perpendicular to the y direction. The control system is assumed to generate a torque u acting upon the hub, a torque u_{tip} and a force f_{tip}

Table 1 Configuration parameters of three-body problem

Parameter	Symbol	Value
Hub radius	r	1 ft
Rotary inertia of hub	J_h	8 slug-ft^2
Mass density of beam	ρ	0.0271875 slug/ft
Elastic modulus of beam	E	0.1584×10^{10} lb/ft^2
Beam length	L	4.0 ft
Moment of inertia of beam	I	$0.4709502797 \times 10^{-7}$ ft^4
Tip mass	m_t	0.156941 slug
Rotary inertia of tip mass	J_t	0.0018 slug-ft^2

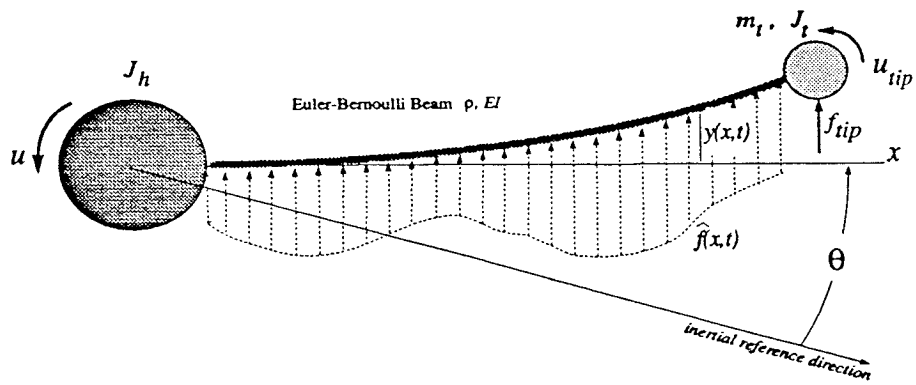

Fig. 4 Three-body distributed-parameter system.

acting upon the tip mass, and a distributed force density $\hat{f}$ acting upon the appendage. We assume small elastic motions viewed from the hub-fixed rotating reference frame. Overdots denote derivatives with respect to time and primes denote derivatives with respect to the spatial position.

The kinetic and potential energies of this hybrid system are as follows:

$$2T = J_h\dot{\theta}^2 + \int_0^L \{\rho[\dot{y} + (x+r)\dot{\theta}]^2\}\,dx + m_t[\dot{y}(L) + (r+L)\dot{\theta}]^2 + J_t[\dot{\theta} + \dot{y}'(L)]^2 \tag{9}$$

$$2V = \int_0^L [EI(y'')^2]\,dx \tag{10}$$

The nonconservative virtual work of this system is given by

$$\delta W_{nc} = \left[u + \int_0^L \hat{f}(x)(x+r)\,dx + (L+r)f_{tip} + u_{tip}\right]\delta\theta + \int_0^L \hat{f}(x)\,\delta y\,dx + f_{tip}\delta y(L) + u_{tip}\delta y'(L) \tag{11}$$

Using an explicit version of the classical Lagrange equation for hybrid coordinate distributed-parameter systems,[12] the governing differential equations and the boundary conditions are obtained efficiently:

$$J_h\ddot{\theta} + \int_0^L \rho(x+r)[\ddot{y} + (x+r)\ddot{\theta}]\,dx + m_t(L+r)[(L+r)\ddot{\theta} + \ddot{y}(L)] + J_t[\ddot{\theta} + \ddot{y}'(L)] = u + \int_0^L \hat{f}(x)(x+r)\,dx + (L+r)f_{tip} + u_{tip} \tag{12}$$

$$\rho[\ddot{y} + (x+r)\ddot{\theta}] + EI\,y'''' = \hat{f} \tag{13}$$

$$EI\frac{\partial^3 y}{\partial x^3}\bigg|_L - m_t[(L+r)\ddot{\theta} + \ddot{y}(L)] + f_{tip} = 0 \tag{14}$$

$$EI\frac{\partial^2 y}{\partial x^2}\bigg|_L + J_t[\ddot{\theta} + \ddot{y}'(L)] - u_{tip} = 0 \tag{15}$$

Notice that if we knew an explicit, differentiable solution for the motion variables $\{y(x,t), \theta(t)\}$, then Eqs. (12–15) can be solved directly and exactly for the four corresponding time and space varying forces and moments $\{u(t), \hat{f}(x,t), u_{tip}(t), f_{tip}(t)\}$, thus yielding the desired inverse solution. Since we are interested in physically meaningful problems, we do not wish to randomly guess the solution $\{y(x,t), \theta(t)\}$. Motivated by the above results for ODEs, we will construct an exact solution that is a near neighbor of a given approximate solution. First we consider a conventional path to construct the approximate solution.

Finite Element Approach

Using the finite element model (FEM), the PDEs of the motion are transformed into an approximate set of second-order differential equations in terms of the displacements, velocities, and accelerations of the finite element coordinates and the external forcing functions. Several FEMs for a flexible arm are presented in Refs. 13 and 14. In this section, we will develop a FEM for a hub with an appendage and a tip mass by using the extended Hamilton principle that provides a variational weak form for the FEM. It is significant to note that we carefully introduce the finite element approximations in such a way that large hub rotations are admitted; the FEM represents small elastic displacements with respect to the hub-fixed axis.

The application of the extended Hamilton principle yields

$$\int_{t_1}^{t_2} (\delta T - \delta V + \delta W_{nc})\,dt = 0, \qquad \delta\theta = \delta y = 0 \quad \text{at} \quad t = t_1, t_2 \tag{16}$$

Substituting Eqs. (9–11) into Eq. (16) and integrating by parts give

$$\int_{t_1}^{t_2}\left(\int_0^L \left\{\rho[\ddot{y} + (x+r)\ddot{\theta}]\,\delta y + EI\frac{\partial^2 y}{\partial x^2}\delta\frac{\partial^2 y}{\partial x^2} - \hat{f}\,\delta y\right\}dx + \left[\int_0^L \rho(x+r)[\ddot{y} + (x+r)\ddot{\theta}]\,dx + J_h\ddot{\theta} + m_t(L+r) \times [\ddot{y}(L) + (L+r)\ddot{\theta}] + J_t\left(\frac{\partial \ddot{y}}{\partial x}\bigg|_L + \ddot{\theta}\right) - \left(u + \int_0^L \hat{f}(x)(x+r)\,dx + (L+r)f_{tip} + u_{tip}\right)\right]\delta\theta + \{m_t[\ddot{y}(L) + (L+r)\ddot{\theta}] - f_{tip}\}\,\delta y(L) + \left[J_t\left(\frac{\partial \ddot{y}}{\partial x}\bigg|_L + \ddot{\theta}\right) - u_{tip}\right]\delta\left(\frac{\partial y}{\partial x}\bigg|_L\right)\right)dt = 0 \tag{17}$$

The displacement $y(x,t)$ can be discretized using a finite element expansion[15,16]:

$$y(x,t) = \sum_{i=1}^{4} \psi_i^{(e)}(x)\nu_i^{(e)}(t) \tag{18}$$

where $\nu_1^{(e)}$, $\nu_2^{(e)}$ ($\nu_3^{(e)}$, $\nu_4^{(e)}$) are transverse deflection and rotation at the left (right) end of the element and $\psi_i^{(e)}$ are the Hermite cubic polynomial shape functions that satisfy the conditions for the admissibility and are defined over the finite element.

The acceleration and curvature are expressed as

$$\ddot{y}(x,t) = \sum_{i=1}^{4} \psi_i^{(e)}(x)\ddot{\nu}_i^{(e)}(t), \qquad \frac{\partial^2 y}{\partial x^2} = \sum_{i=1}^{4} \frac{\partial^2}{\partial x^2}\left[\psi_i^{(e)}(x)\right]\nu_i^{(e)}(t) \tag{19}$$

The following cubic functions are adopted as the shape functions for ith finite element[16]:

$$\psi_1 = 1 - 3\bar{x}_i^2 + 2\bar{x}_i^3, \qquad \psi_2 = h\bar{x}_i - 2h\bar{x}_i^2 + h\bar{x}_i^3$$
$$\psi_3 = 3\bar{x}_i^2 - 2\bar{x}_i^3, \qquad \psi_4 = -h\bar{x}_i^2 + h\bar{x}_i^3, \qquad \bar{x}_i \equiv (x - x_i)/h \tag{20}$$

where x_i is the distance from the root of the appendage to the left end of the ith finite element and h is the length of the finite element. These are the most commonly used shape functions for one-dimensional beam elements.

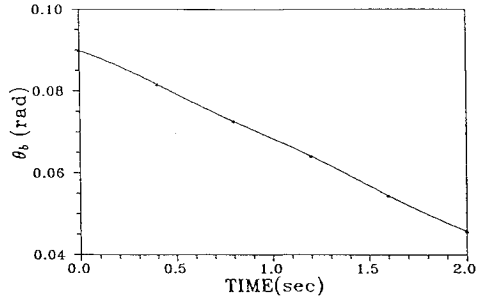

Fig. 5 Hub rotation angle $\theta_b(t)$.

Substitution of Eqs. (18–20) into Eq. (17) and carrying out the spatial integrations yield the global mass, stiffness, and forcing matrices. After some algebra, the assembled matrix differential equation is

$$\begin{bmatrix} J_h + M_{\theta\theta} & M_{\theta\nu} \\ M_{\nu\theta} & M_{\nu\nu} \end{bmatrix} \begin{Bmatrix} \ddot{\theta} \\ \ddot{\nu} \end{Bmatrix} + \begin{bmatrix} 0 & 0 \\ 0 & K_{\nu\nu} \end{bmatrix} \begin{Bmatrix} \theta \\ \nu \end{Bmatrix}$$

$$= \begin{bmatrix} 1 & r+L & 1 \\ 0 & 0 & 0 \\ \vdots & \vdots & \vdots \\ 0 & 1 & 0 \\ 0 & 0 & 1 \end{bmatrix} \begin{Bmatrix} u \\ f_{\text{tip}} \\ u_{\text{tip}} \end{Bmatrix}$$

$$+ \begin{bmatrix} \int_0^L \hat{f}(x)(x+r)\,dx \\ \int_0^h \hat{f}(x)\psi_3^{(1)}(x)\,dx + \int_h^{2h} \hat{f}(x)\psi_1^{(2)}(x)\,dx \\ \int_0^h \hat{f}(x)\psi_4^{(1)}(x)\,dx + \int_h^{2h} \hat{f}(x)\psi_2^{(2)}(x)\,dx \\ \vdots \\ \int_{(l-2)h}^{(l-1)h} \hat{f}(x)\psi_4^{(l-1)}(x)\,dx + \int_{(l-1)h}^{lh} \hat{f}(x)\psi_2^{(l)}(x)\,dx \\ \int_{(l-1)h}^{lh} \hat{f}(x)\psi_3^{(l)}(x)\,dx \\ \int_{(l-1)h}^{lh} \hat{f}(x)\psi_4^{(l)}(x)\,dx \end{bmatrix} \tag{21}$$

where ν is the coordinate that consists of the transverse deflection and rotation at each node of the appendage and l is the number of finite elements. The matrix elements of Eq. (21) are presented in Ref. 8.

Construction of Candidate Discrete Solution

We can find a physically meaningful approximate solution by using any given approximate forward solution process. For simplicity, we assume that only the hub torque $u(t)$ is nonzero. Then Eq. (21) can be written in a linear second-order matrix form as

$$M\ddot{x} + Kx = \begin{bmatrix} 1 \\ \mathbf{0} \end{bmatrix} u \qquad \text{where} \qquad x = \begin{Bmatrix} \theta \\ \nu \end{Bmatrix} \tag{22}$$

We design a typical control law using the LQR, and modal coordinates[17] are used to design controller. For control applications the system dynamics are usually modeled as first-order state-space differential equations.[8] Equation (22) can be written as the first-order system $\dot{z} = Az + Bu$, where z is the modal state vector.

We adopted the following performance index for the LQR control design:

$$J = \int_0^\infty (z^T Qz + u^T Ru)\,dt \quad \text{with} \quad Q = \begin{bmatrix} \Omega & 0 \\ 0 & I_n \end{bmatrix}, \quad R = 1 \tag{23}$$

where $\Omega = \text{diag}(q, \omega_1^2, \ldots, \omega_{n-1}^2)$ and ω_i is the natural frequency of the ith flexible mode.

The above performance index is an energy type, since the first term and second term in the performance index correspond to the state energy and the control energy, respectively.

The optimal feedback control is obtained by solving the Riccati equation.[18]

Now we can solve the initial-value problem using a time discretization process (e.g., Runge-Kutta) and then we obtain $\tilde{y}(x_i, t_i)$, $\tilde{\theta}(t_i)$, and $\tilde{u}(t_i)$ at discrete points in space and time. The approximate motion $\{\tilde{y}(x_i, t_i), \tilde{\theta}(t_i)\}$ corresponds to the system response to a hub torque designed to maneuver the system and arrest vibration.

Construction of Benchmark Problem

We want to construct a continuous, differentiable, analytical solution that has physical meaning. A candidate discrete approximate solution for the hybrid system can be obtained using any given approximate forward solution process and a given controller. This approximate solution can be used as a generator for a nearby smooth space-time motion for which we can determine the exact forces (required to be consistent with this prescribed motion and the exact equations of motion). Least-squares approximation associated with using the discrete version of the Chebyshev polynomials can be invoked to obtain the smooth $f(x, y)$ solution from the discrete solution. Whereas we invoke a least-squares approximation to construct the smooth $f(x, y)$ from an already approximate discrete solution, we subsequently determine the modified forces to be exactly consistent with this motion $f(x, y)$. We first consider the least-squares process.

There are $n' \times m'$ discrete data points such as

$$z_{11} = f(x_1, y_1),\ z_{12} = f(x_1, y_2), \ldots, z_{1m'} = f(x_1, y_{m'})$$

$$z_{21} = f(x_2, y_1),\ z_{22} = f(x_2, y_2), \ldots, z_{2m'} = f(x_2, y_{m'})$$

$$\vdots$$

$$z_{n'1} = f(x_{n'}, y_1),\ z_{n'2} = f(x_{n'}, y_2), \ldots, z_{n'm'} = f(x_{n'}, y_{m'})$$

where x_i, y_j are equally spaced independent variables.

How can we reliably compute a continuous, differentiable, analytical function f from the data points in the least-squares sense? Analogous to the ODE case, we elect to make use of discrete orthogonality. We nondimensionalize (x, y) using

$$\bar{x}(x) = \frac{x - x_1}{h_x}, \qquad \bar{y}(y) = \frac{y - y_1}{h_y}$$

where h_x, h_y are the increments of x and y, respectively:

$$z = f(x, y) = F(\bar{x}, \bar{y})$$

From two-dimensional $n' \times m'$ data points, the function F can be approximated by $p \times q$ two-dimensional basis functions that come from the discrete version of the Chebyshev polynomials [weight function $w(x) = 1$] as follows:

$$F(\bar{x}, \bar{y}) \equiv \sum_{i=1}^{p} \sum_{j=1}^{q} b_{ij} T_i(\bar{x}) T_j(\bar{y})$$

where $p \le n'$, $q \le m'$ and $T_*(*)$ is the univariate Chebyshev polynomial in the discrete range.[7,8]

We use the conventional definitions of Chebyshev polynomials and the corresponding recurrence relations.[8] Using discrete orthogonality properties of Chebyshev polynomials, the typical coefficient b_{rs} can be obtained as

$$b_{rs} = \frac{\sum_{i=1}^{n'} \sum_{j=1}^{m'} z_{ij}\, T_r(\bar{x}_i)\, T_s(\bar{y}_j)}{\sum_{i=1}^{n'} \sum_{j=1}^{m'} T_r(\bar{x}_i)\, T_s(\bar{y}_j)\, T_r(\bar{x}_i)\, T_s(\bar{y}_j)}$$

where $1 \le r \le p$, $1 \le s \le q$.

We can find $f(x, y)$ from $F(\bar{x}, \bar{y})$, since $f(x, y) = F(\bar{x}(x), \bar{y}(y))$.

Using the above approximation method, we interpolate a smooth differentiable function $y_b(x, t)$ as a two-variable orthogonal function expansion that passes near the $\tilde{y}(x_i, t_i)$ points. Similary, we can interpolate a smooth differentiable function $\theta_b(t)$ from $\tilde{\theta}(t_i)$ data points. Since $y_b(x, t)$ and $\theta_b(t)$ are smooth, differentiable functions, we can force them to be exact solutions of our dynamic model by simply substituting $y_b(x, t)$, $\theta_b(t)$ and their space-time derivatives into Eqs. (12–15) and solving the four equations analytically for four corresponding forces $\{u(t), \hat{f}(x, t), u_{\text{tip}}(t), f_{\text{tip}}(t)\}$ that satisfy these equations exactly. Computer symbol manipulation makes this process practical.

Simulated Results

First we find a candidate discrete solution for the enlarged time interval $(-1 \le t \le 2)$ with initial conditions $\theta(-1) = 0.1$ rad and $y(x, -1) = 0$ for all x. We use the LQR algorithm to design control force $\tilde{u}(t)$ and use the finite element approach for space discretization. Here we use 1 for q of Eq. (23) and use

the configuration parameters shown in Table 1. Then we construct a benchmark problem for time interval $0 \leq t \leq 2$. Figures 5–10 show $y_b(x,t)$, $\theta_b(t)$, $u(t)$, $\hat{f}(x,t)$, $u_{\text{tip}}(t)$, and $f_{\text{tip}}(t)$ that satisfy Eqs. (12–15) exactly. Note that even though we use the enlarged time interval and have good approximations for $\theta_b(t)$ and $y_b(x,t)$ near the boundary, there may exist relatively large errors for control forces, near the boundary, compared to the nonlinear ODE cases. This is due to the fact that we have two independent variables, time and space, and have coupling terms that depend upon time and space derivatives of $y_b(x,t)$ in the evaluation of control forces. Also, in contrast to enlarging the time interval for ODE problems, it is neither physically nor mathematically meaningful to enlarge the spatial domain. As will be evident, this is a minor problem and does not prevent us from establishing "exact" benchmark problems.

The finite element approach gives us Eq. (21), and for simulation we generate a step-by-step solution using the Newmark integration method. Given initial conditions $\{y(x,0) = y_b(x,0), \theta(0) = \theta_b(0)\}$ and force functions $\{u(t), \hat{f}(x,t), u_{\text{tip}}(t), f_{\text{tip}}(t)\}$, the approximate simulation of this structure's dynamics $\{y_s(x,t), \theta_s(t)\}$ can proceed. Figure 11 shows the space-time error distribution $e_y(x,t) = y_s(x,t) - y_b(x,t)$ when we use 20 finite elements and 0.002 s for step size.

Second, we find a candidate solution for the enlarged time interval $0 \leq t \leq 0.1$. The initial condition for θ is 0.1 rad, and the third natural mode of this flexible structure is used for the initial deformation $y(x,0)$. We use the LQR algorithm to design control force $\tilde{u}(t)$ and the FEM is used for spatial discretization. Here we use 100 for q of Eq. (23) and use the configuration parameters shown Table 1 except m_t and J_t ($m_t = 0.256941$, $J_t = 0.0028$). Then we construct a benchmark problem for time interval $0 \leq t \leq 0.08$; i.e., we have new set $y_b(x,t)$, $\theta_b(t)$ and $\{u(t), \hat{f}(x,t), u_{\text{tip}}(t), f_{\text{tip}}(t)\}$ that satisfy Eqs. (12–15) exactly.

Now we can investigate the convergence errors in a family of approximate solutions with the special case providing an absolute standard. When we use the Newmark integration method with finite element modeling, the convergence and accuracy behavior is studied as a function of the number of finite elements and the integration step size. Figure 12 shows the error norms $\|e_\theta\|$ and $\|e_y\|$ for various mesh sizes for a fixed integration step size on a log-log scale. Figure 13 shows the error norms $\|e_\theta\|$ and $\|e_y\|$ for various integration step sizes for a fixed number of finite elements on a log-log scale. The error norm distribution of θ and y is shown in Figs. 14 and 15, respectively, as a function of DT (time step size) and H (mesh size).

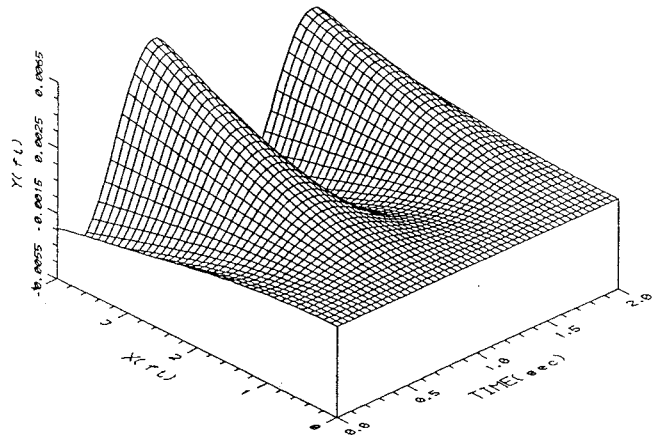

Fig. 6 Elastic displacement $y_b(x,t)$.

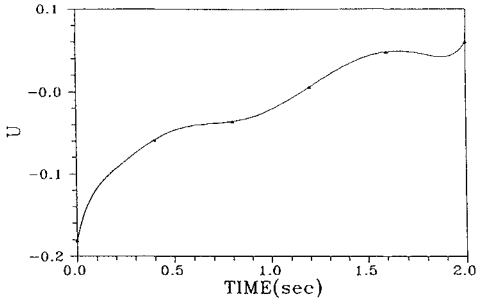

Fig. 7 Hub control $u(t)$.

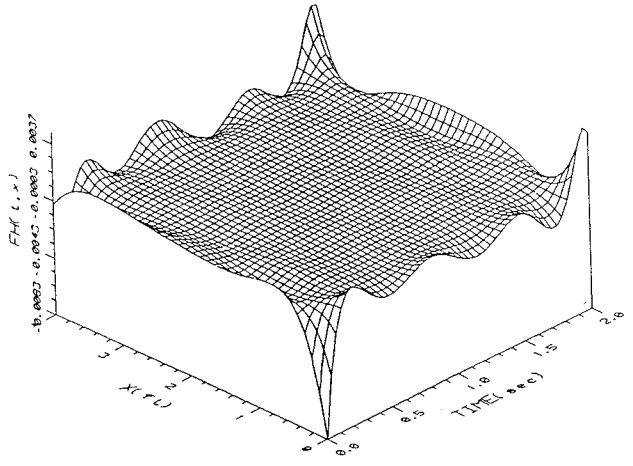

Fig. 8 Distributed force density $\hat{f}(x,t)$.

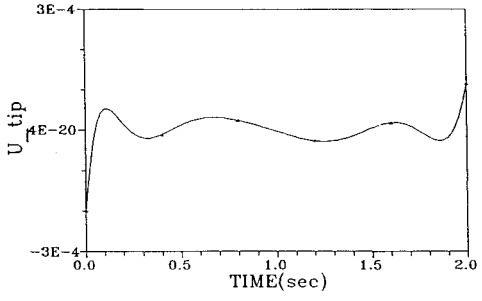

Fig. 9 Torque applied at tip $u_{\text{tip}}(t)$.

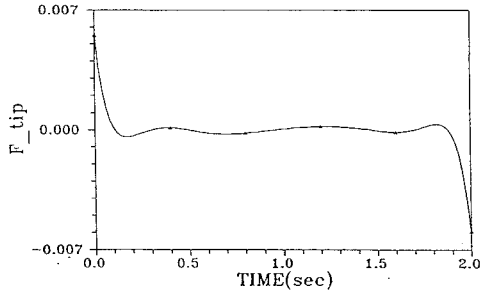

Fig. 10 Force applied at tip $f_{\text{tip}}(t)$.

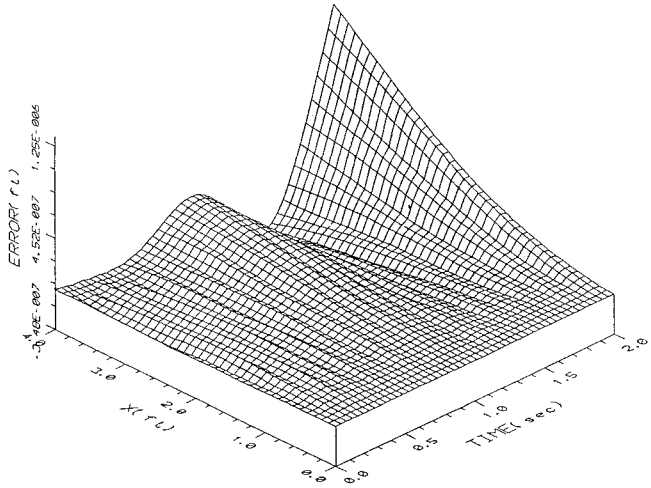

Fig. 11 Error distribution $e_y(x,t) = y_s(x,t) - y_b(x,t)$.

Here we introduce the following definitions for the supmetric error:

$$\|e_\theta(t)\|_{L^2(0,T)} \equiv \left[\int_0^T e_\theta(t)^2 dt\right]^{1/2}$$

$$\|e_y(x,t)\|_{L^2(0,T;L^2)} \equiv \left[\int_0^T \int_0^L e_y(x,t)^2\, dx\, dt\right]^{1/2}$$

where $e_\theta(t) = \theta_s(t) - \theta_b(t)$.

The relative errors are defined as

$$\mathrm{RE}_\theta \equiv \frac{\|e_\theta(t)\|_{L^2(0,T)}}{\|\theta(t)\|_{L^2(0,T)}}, \qquad \mathrm{RE}_y \equiv \frac{\|e_y(x,t)\|_{L^2(0,T;L^2)}}{\|y(x,t)\|_{L^2(0,T;L^2)}}$$

We observe that the rate of convergence is 2 in DT and 4 in H from Figs. 12 and 13, except for the small (DT, H) region where arithmetic errors dominate and provide us visibility of algorithm and especially computer limitations to accuracy. It is this latter insight that is essentially impossible to obtain by pre-existing methods but is easily established by the methods of this paper. We should be careful in saying that adjusting H (to achieve accuracy) is less expensive than adjusting DT, because the rate of convergence of 4 in H and the rate of convergence of 2 in DT do not guarantee this fact. Each approach to improving accuracy results in a different amount of computational load, which depends on the specific program. From Figs. 12–15, we can also notice that if H is too crude, then DT reduction does not improve the solution, and if DT is too big, then H reduction does not improve the solution. The numerical results indicate that the minimum value of RE_θ is 0.7×10^{-7} (when $H = 0.2$ and DT = 0.00002) and the minimum value of RE_y is 0.3×10^{-3} (when $H = 0.4$ and DT = 0.00005). We know of no method that could give this insight before the introduction of the present method.

Finally, we construct a neighboring benchmark problem to investigate the robustness of the convergence characteristics of Figs. 12–15. To construct a neighboring benchmark problem, first we find a candidate discrete solution with the following initial condition and forcing function $\tilde{u}(t)$. Comparing to the previous case, we make a 10% increase of the initial condition $y(x, 0)$ and arbitrarily add a sinusoidal perturbation term $0.4186\sin(2\pi t/0.08)$ to the previous

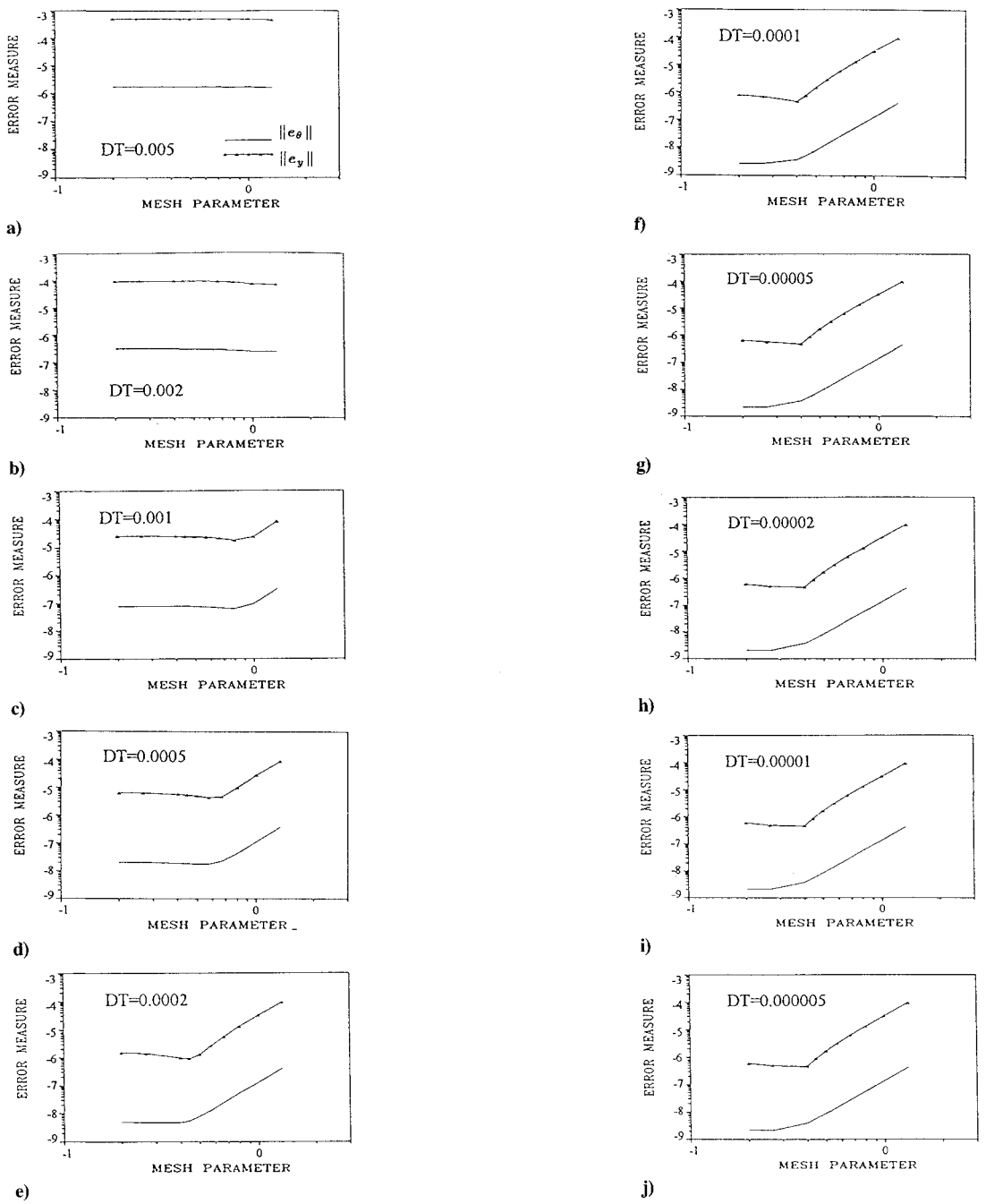

Fig. 12 Error norms for various mesh sizes for fixed integration step size.

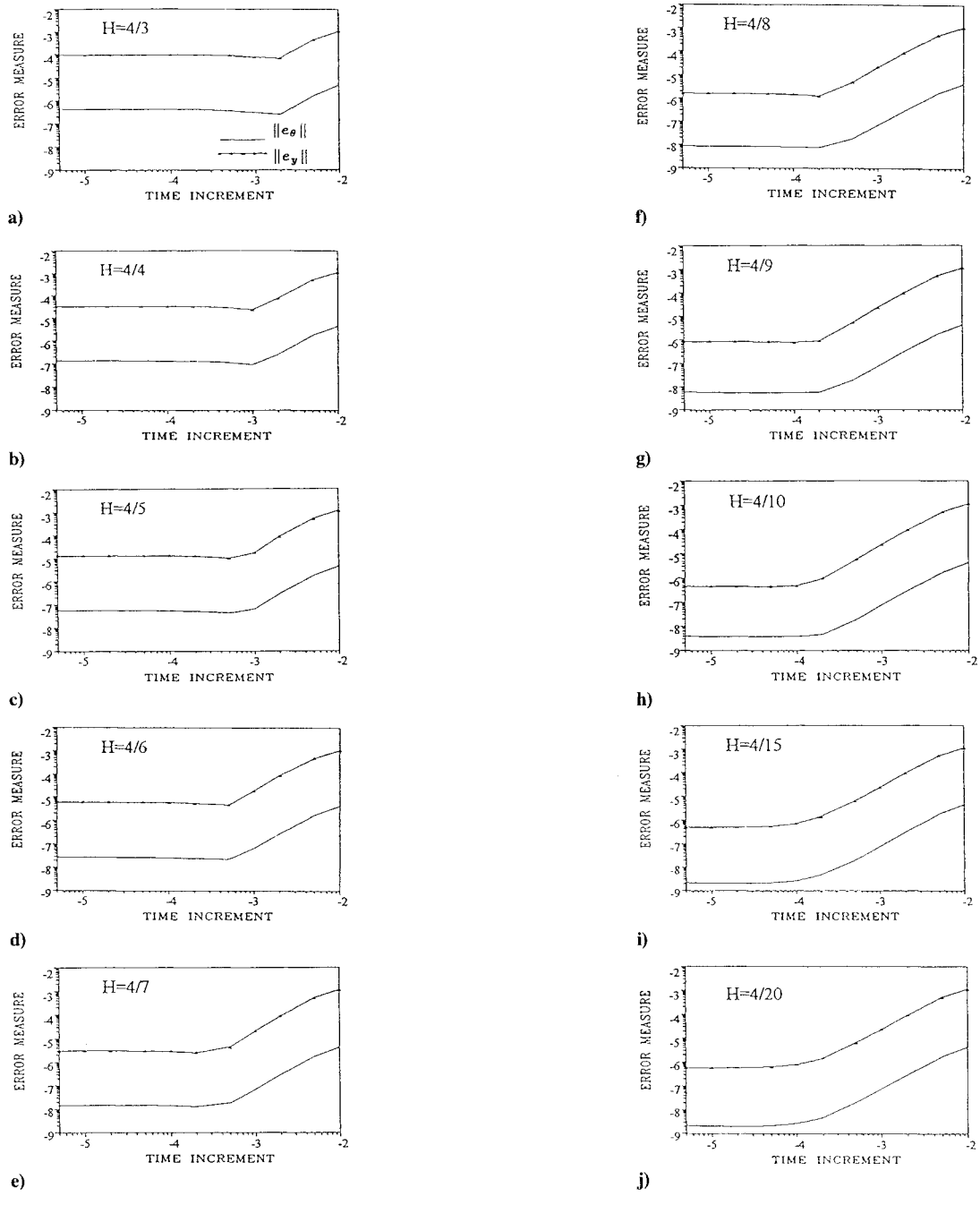

Fig. 13 Error norms for various integration step sizes for fixed mesh size.

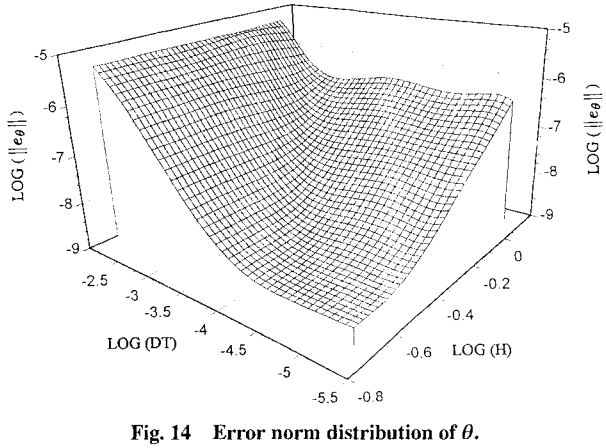

Fig. 14 Error norm distribution of θ.

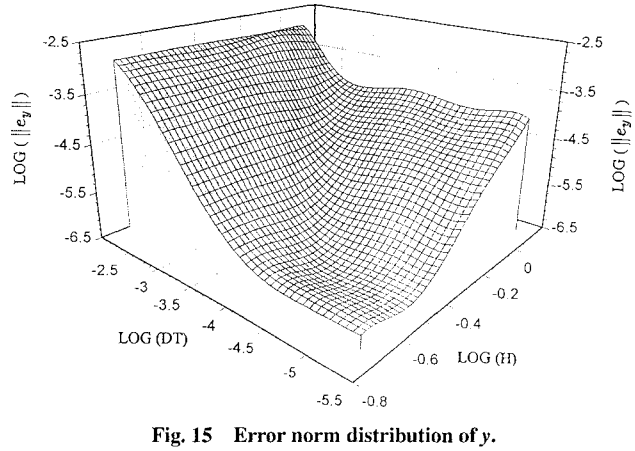

Fig. 15 Error norm distribution of y.

hub control $\tilde{u}(t)$ for a new perturbed hub control. The error norm distributions of the perturbed case are found to be almost identical to the previous problem. So we can conclude that the convergence and accuracy properties of this approximate solution process are indeed relatively invariant in the presence of these finite perturbations, in this case.

Summary and Conclusion

The present paper introduces an inverse dynamics method for constructing exact special-case solutions for hybrid ODE/PDE systems. A multivariable orthogonal function expansion method and computer symbol manipulation are successfully used for this process. The hybrid ODE/PDE systems with exact solutions can serve as a benchmark problem to validate approximate solution methods. This methodology makes it possible for one to rigorously determine exact solution errors and to study the convergence and accuracy behavior as a function of tuning parameters for a class of ODE/PDE systems for which the initial-value problem is not exactly solvable. Numerical examples indicate that a rigorous error analysis is obtained, not merely for one nominal solution, but for a substantial neighborhood of the nominal solution. By constructing a family of neighboring benchmark problems, one can obtain valuable information about the convergence and accuracy properties that are relatively invariant with respect to perturbations within a known bound.

References

[1]Lee, S., and Junkins, J. L., "Construction of Benchmark Problems for Solution of Ordinary Differential Equations," *Journal of Shock and Vibration*, Vol. 1, No. 5, 1994, pp. 403–414.

[2]Shampine, L. F., "Tolerance Proportionality in ODE Codes," *Numerical Methods for Ordinary Differential Equations*, edited by A. Bellen, C. W. Gear, and E. Russo, Springer-Verlag, Berlin, 1987, pp. 118–135.

[3]Hairer, E., Norsett, S. P., and Wanner, G., *Solving Ordinary Differential Equations, Vol. I: Nonstiff Problems*, Springer-Verlag, Berlin, 1987.

[4]Hull, T. E., Enright, W. H., Fellen, B. M., and Sedgwick, A. E., "Comparing Numerical Methods for Ordinary Differential Equations," *SIAM Journal of Numerical Analysis*, Vol. 9, No. 4, 1972, pp. 603–637.

[5]Krogh, F. T., "On Testing a Subroutine for the Numerical Integration of Ordinary Differential Equations," *Journal of the Association for Computing Machinery*, Vol. 20, No. 4, 1973, pp. 545–562.

[6]Junkins, J. L., *An Introduction to Optimal Estimation of Dynamical Systems*, Sijhoff & Noordhoff, Alphen aan den Rijn, The Netherlands, 1978.

[7]Abramowitz, M., and Stegun, I. A., *Handbook of Mathematical Functions with Formulas, Graphs, and Mathmatical Tables*, National Bureau of Standards, Applied Mathematics Series 55, U.S. Department of Commerce, Washington, DC, 1972.

[8]Junkins, J. L., and Lee, S., "Validation of Finite Dimensional Approximate Solutions for Dynamics of Distributed Parameter Systems," *Advances in the Astronautical Sciences*, Vol. 85; also AAS Paper 93-641, Aug. 1993.

[9]*MACSYMA Reference Manual Version 13*, Symbolics, 1988.

[10]Gear, C. W., *Numerical Initial Value Problems in Ordinary Differential Equations*, Prentice-Hall, Englewood Cliffs, NJ, 1971.

[11]Bathe, K. J., *Finite Element Procedures in Engineering Analysis*, Prentice-Hall, Englewood Cliffs, NJ, 1982.

[12]Lee, S., and Junkins, J. L., "Explicit Generalization of Lagrange's Equations for Hybrid Coordinate Dynamical Systems," *Journal of Guidance, Control, and Dynamics*, Vol. 15, No. 6, 1992, pp. 1443–1452.

[13]Bayo, E., "A Finite-Element Approach to Control the End-Point Motion of a Single-Link Flexible Robot," *Journal of Robotic Systems*, Vol. 4, No. 1, 1987, pp. 63–75.

[14]Naganathan, G., and Soni, A. H., "Coupling Effects of Kinematics and Flexibility in Manipulators," *International Journal of Robotics Research*, Vol. 6, No. 1, 1987, pp. 75–84.

[15]Reddy, J. N., *An Introduction to the Finite Element Method*, McGraw-Hill, New York, 1984.

[16]Craig, R. R., Jr., *Structural Dynamics—an Introduction to Computer Methods*, Wiley, New York, 1981.

[17]Meirovitch, L., *Computational Methods in Structural Dynamics*, Sijhoff & Noordhoff, The Netherlands, 1980.

[18]Junkins, J. L., and Kim, Y., *An Introduction to Dynamics and Control of Flexible Structures*, AIAA, Washington, DC, 1993.